Supporting Information for

Conductive Wood for High-Performance Structural Electromagnetic Interference Shielding

Wentao Gan,[1a] Chaoji Chen,[1a] Michael Giroux,[2a] Geng Zhong,[1] Mukund Goyal,[2] Yilin Wang,[1] Weiwei Ping,[1] Jianwei Song,[1] Shaomao Xu,[1] Shuaiming He,[1] Miaolun Jiao,[1] Chao Wang,[2*] Liangbing Hu[1,*]

1. Department of Materials Science and Engineering, University of Maryland, College Park, Maryland, 20742
2. Department of Chemical & Biomolecular Engineering, Johns Hopkins University, Baltimore, Maryland, 21218

[*]Email: binghu@umd.edu; chaowang@jhu.edu

[a]These authors contributed equally to this work.

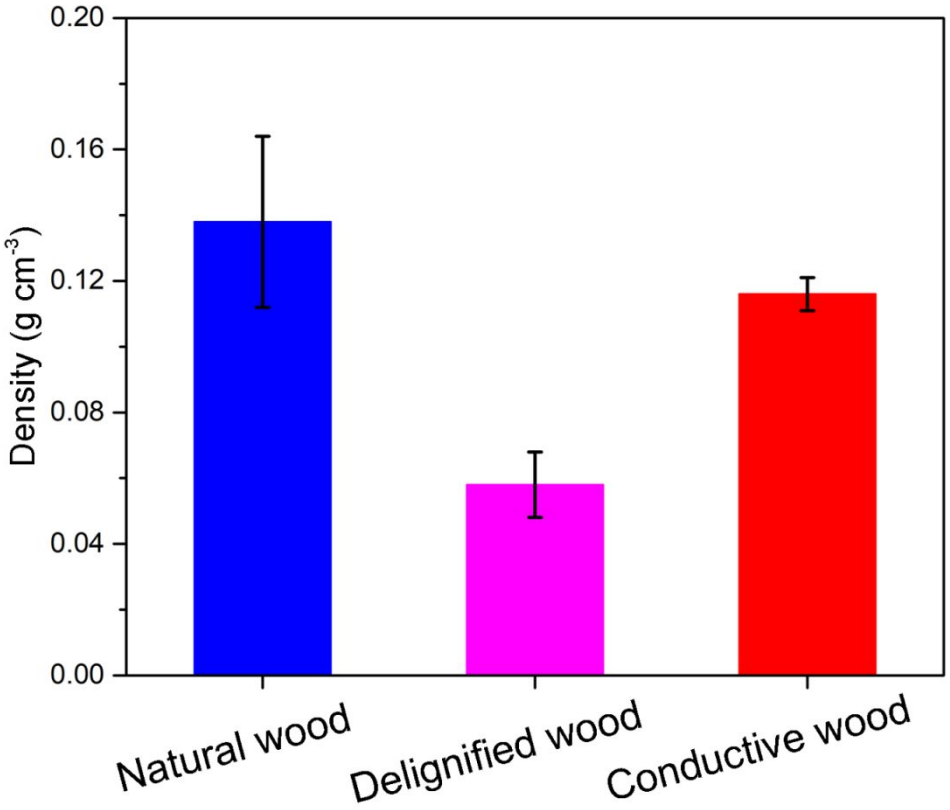

Figure S1. The density of natural wood, delignified wood, and conductive wood. The conductive wood is lightweight, with a density of just 0.11 g cm^{-3}.

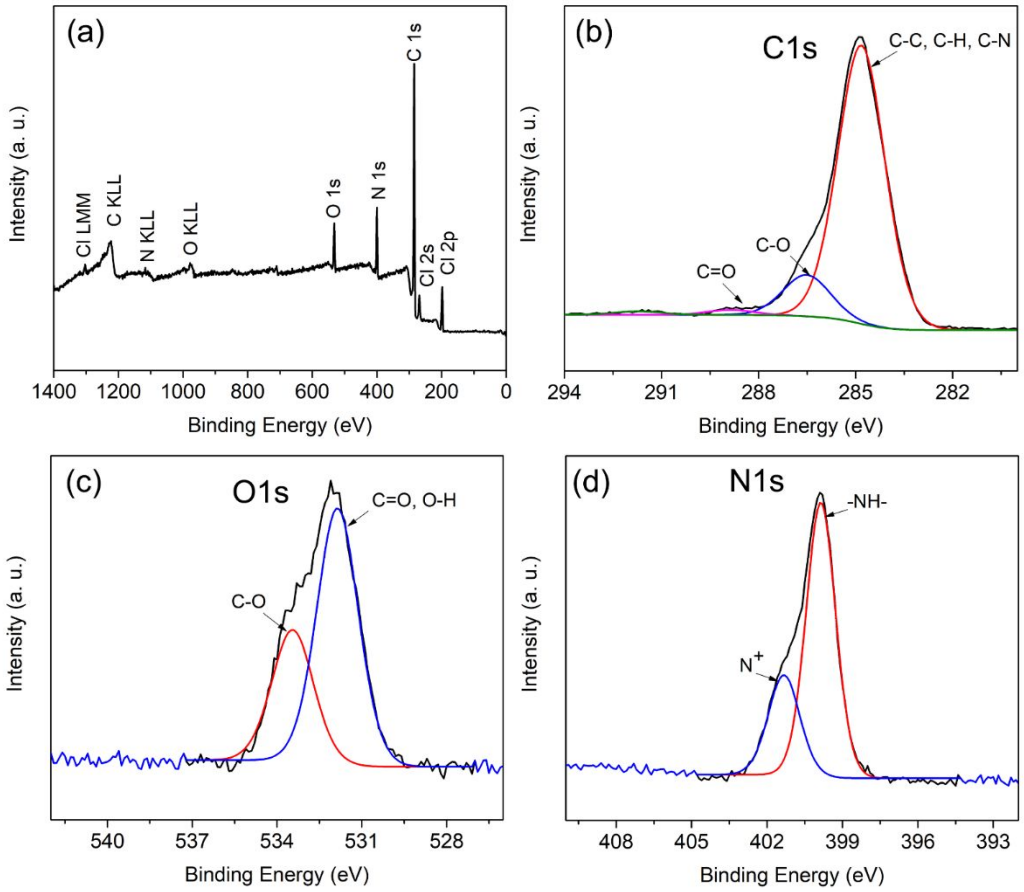

Figure S2. (a) Survey, (b) C 1s, (c) O 1s and (d) N 1s XPS spectra of conductive wood.

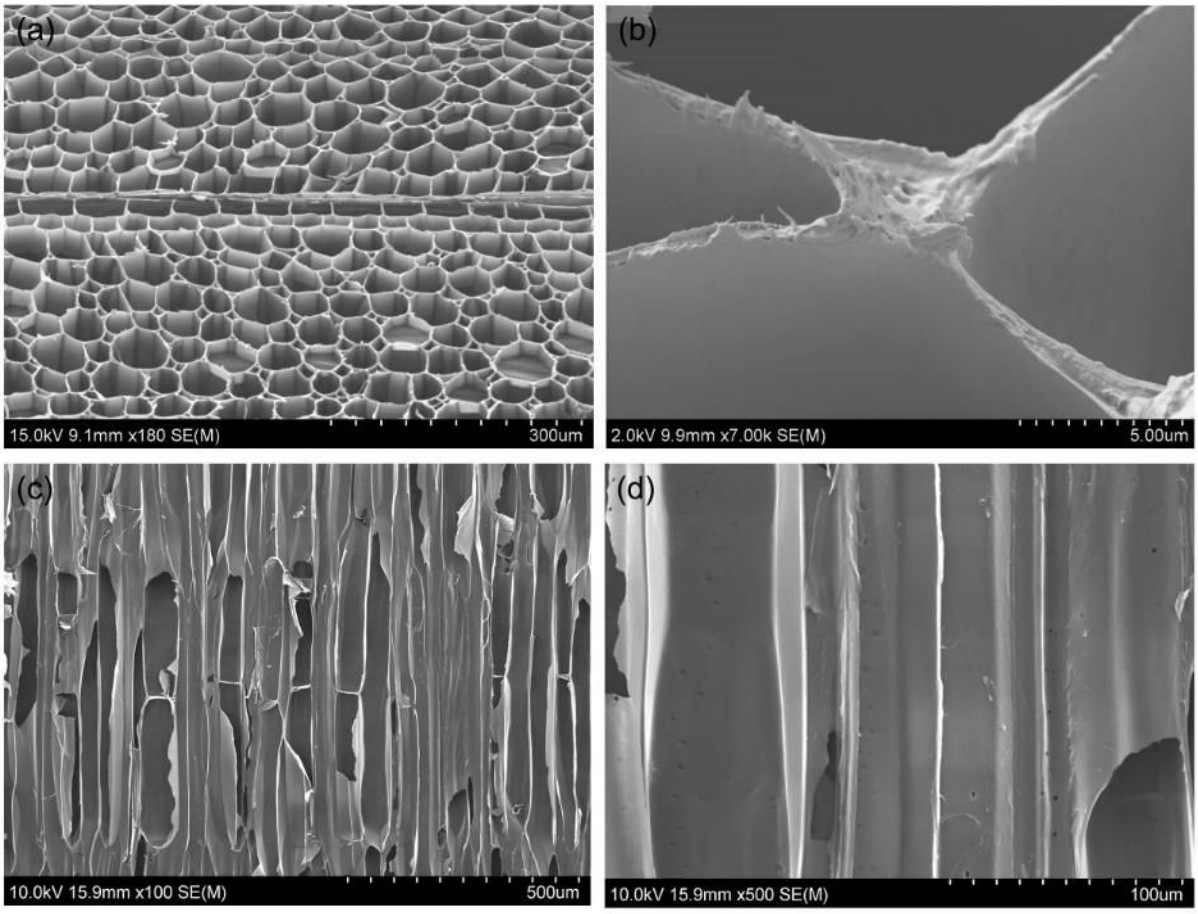

Figure S3. (a, b) Top-view and (c, d) cross-sectional SEM images of natural balsa wood.

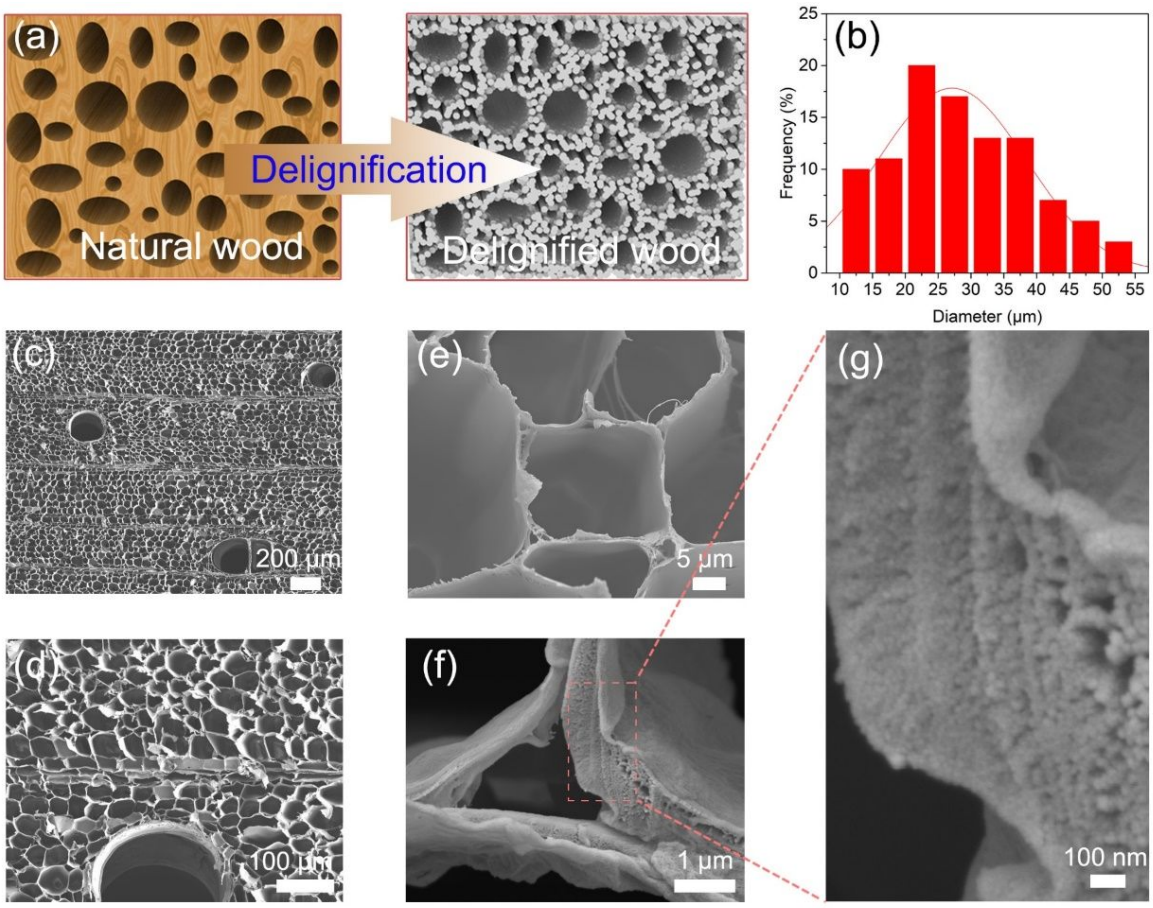

Figure S4. (a) Schematic illustrations of the delignified wood before and after delignification. (b) The diameter distribution of the open delignified wood cell (exclude the maximal pores). (c-f) SEM images of the delignified wood showing the porous structure. (g) High magnification SEM image of the delignified wood shows the cellulose nanofibrils are exposed in the wood cell walls after delignification.

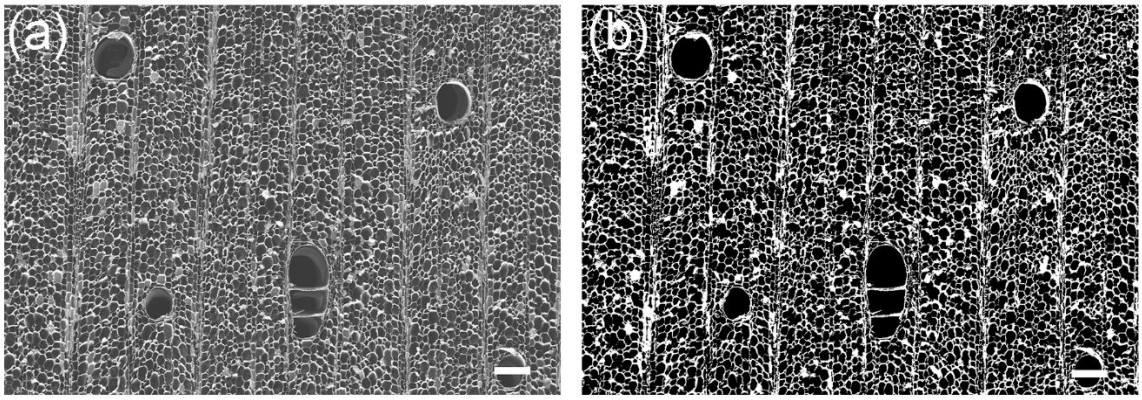

Figure S5 (a) the original SEM of delignified wood, (b) binary image of delignified wood. Scale bar: 300 μm.

The surface porosity of delignified wood is calculated using an image analysis method.[1] The original SEM image was converted to a binary image by setting a threshold of 128, and the porosity of the wood can be calculated as follows:

$$P = n/N \times 100\% \quad (1)$$

where n and N denote the number of black pixels and the total pixels in the binary images, respectively.

According to Figure S5b, the n and N was counted as 211635 and 286080, respectively. Thus, the porosity of delignified wood should be 73.9%.

However, only the large pore volume of wood can be calculated using the Eq. 1. Taking the density of air and cellulose into consideration, the porosity of wood after total delignification including nanopores can be calculated as:

$$\text{Pore volume fraction (\%)} = (1 - \rho(\text{sample})/\rho(\text{cellulose})) \times 100\% \quad (2)$$

where ρ (sample) is 0.058 g/cm^3 (Figure S1), ρ (cellulose) is the cellulose density, which is about 1.5 g/cm^3.

Using the Eq. 2, the porosity of the delignified wood can be calculated to be 96.1%, which is much higher than the result calculated by the image analysis method, indicating a large amount of nanopores present in the delignified wood.

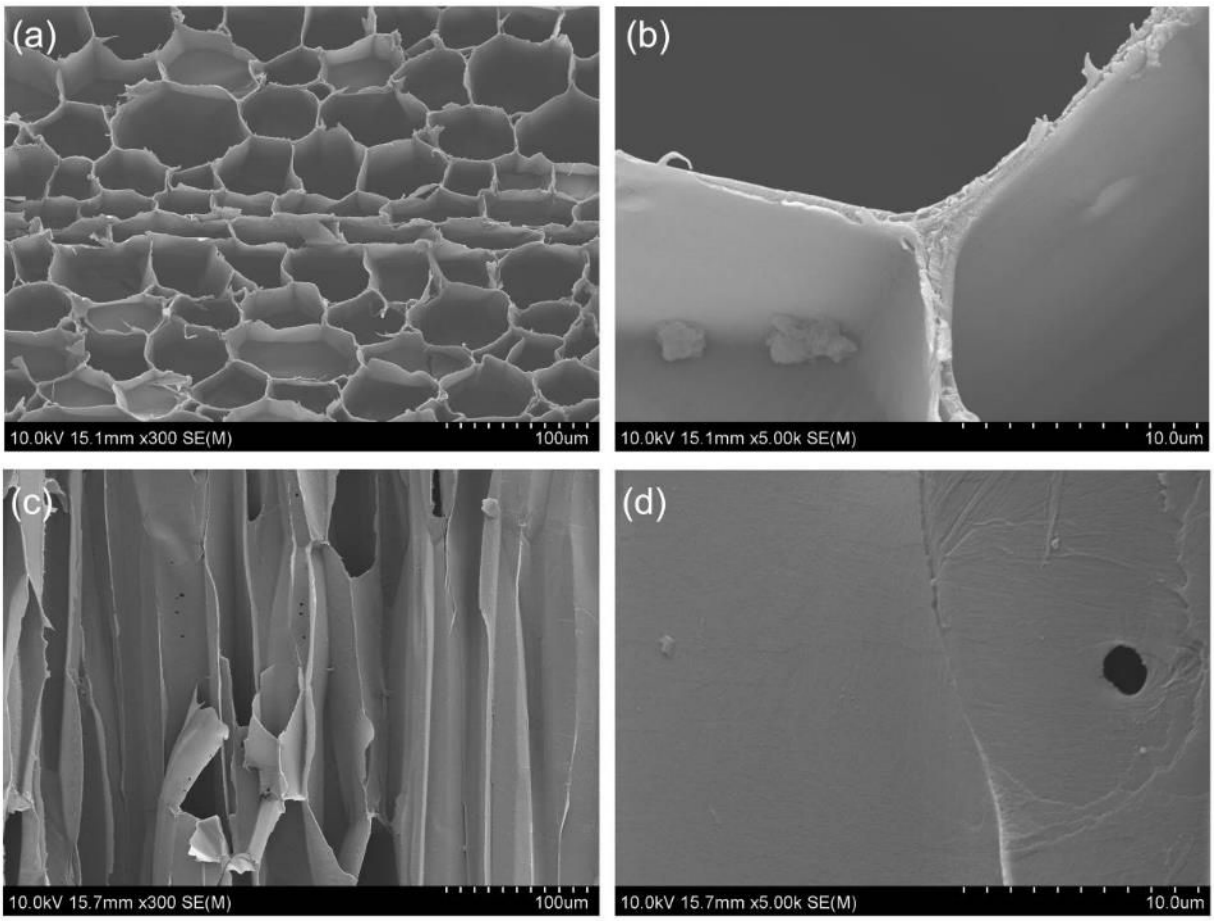

Figure S6. (a, b) Top-view and (c, d) cross-sectional SEM images of natural wood after the $FeCl_3$ treatment. The smooth wood cell walls reveal only a small amount of $FeCl_3$ deposited on the natural wood substrate.

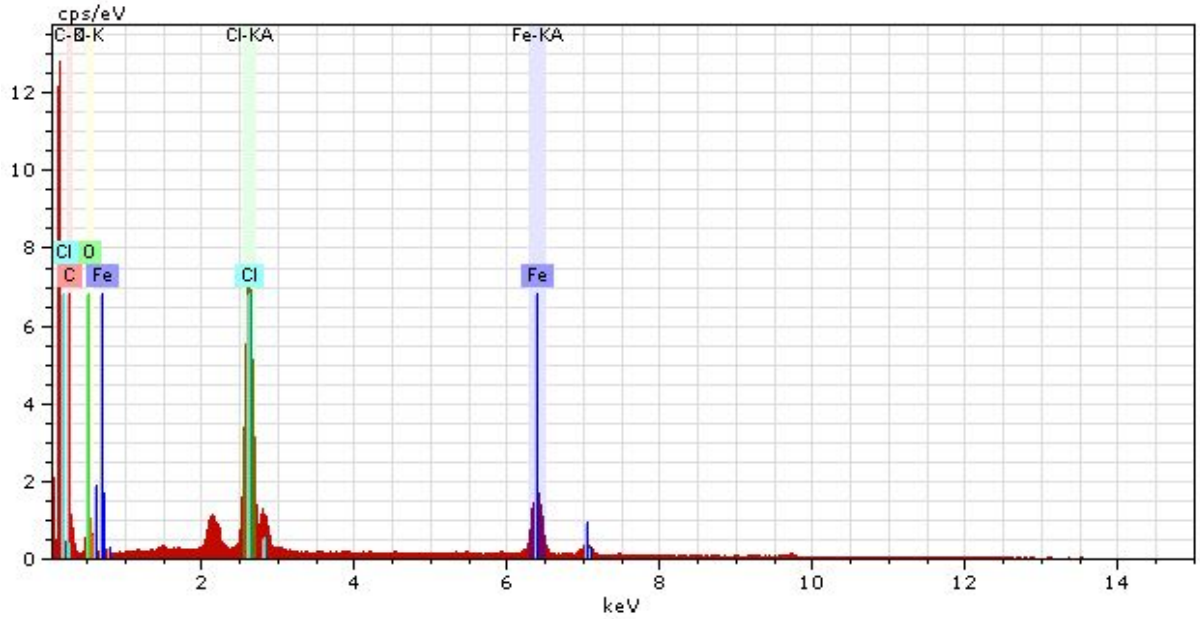

Figure S7. The EDX spectrum of delignified wood after $FeCl_3$ adsorption, indicating a large amount of Fe^{3+} and Cl^- present on the delignified wood substrate.

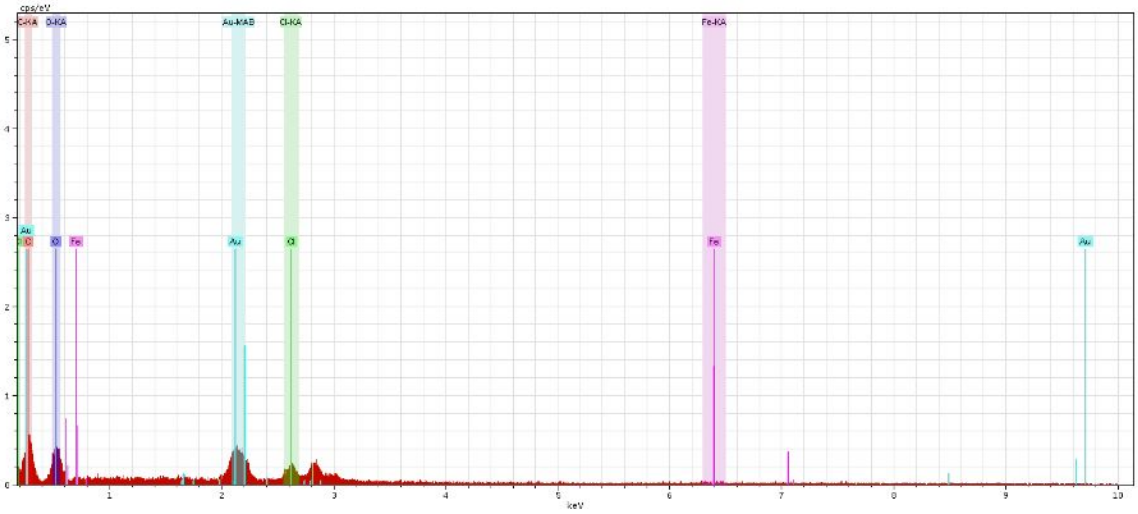

Figure S8. The EDX spectrum of natural wood after the $FeCl_3$ treatment, indicating the low loading of $FeCl_3$.

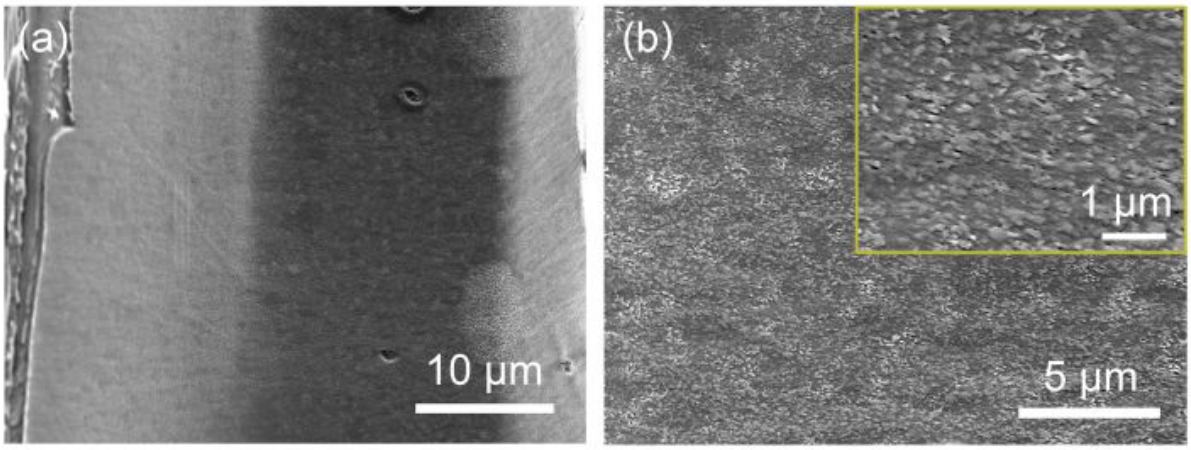

Figure S9. (a, b) Cross-sectional SEM images of the conductive wood show the PPy layer coated on the wood channels.

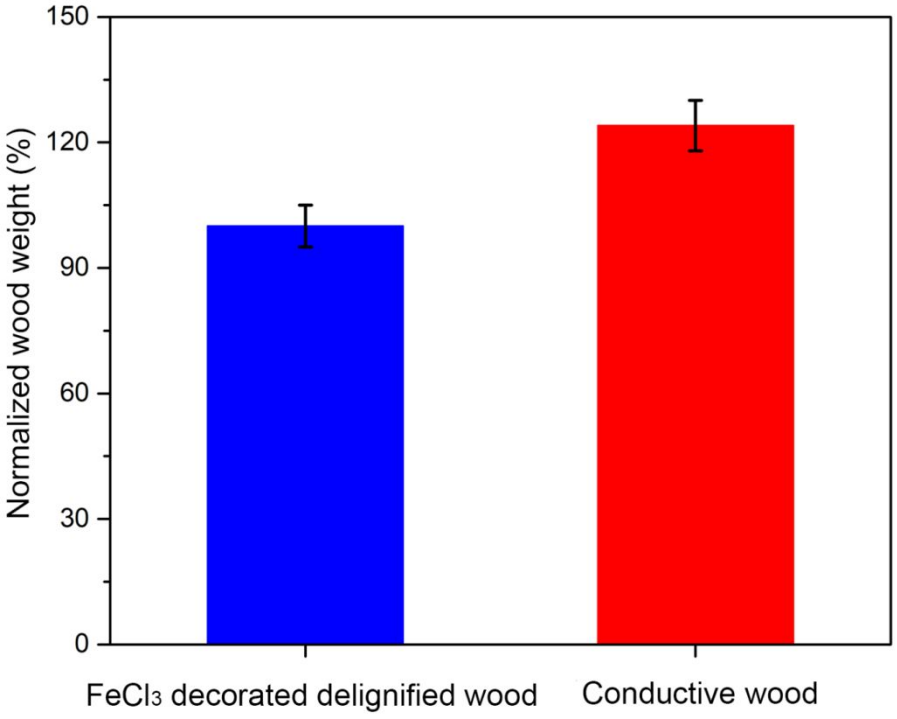

Figure S10. The normalized weight-change before and after the PPy coating shows the conductive wood was loaded with 24 wt% PPy.

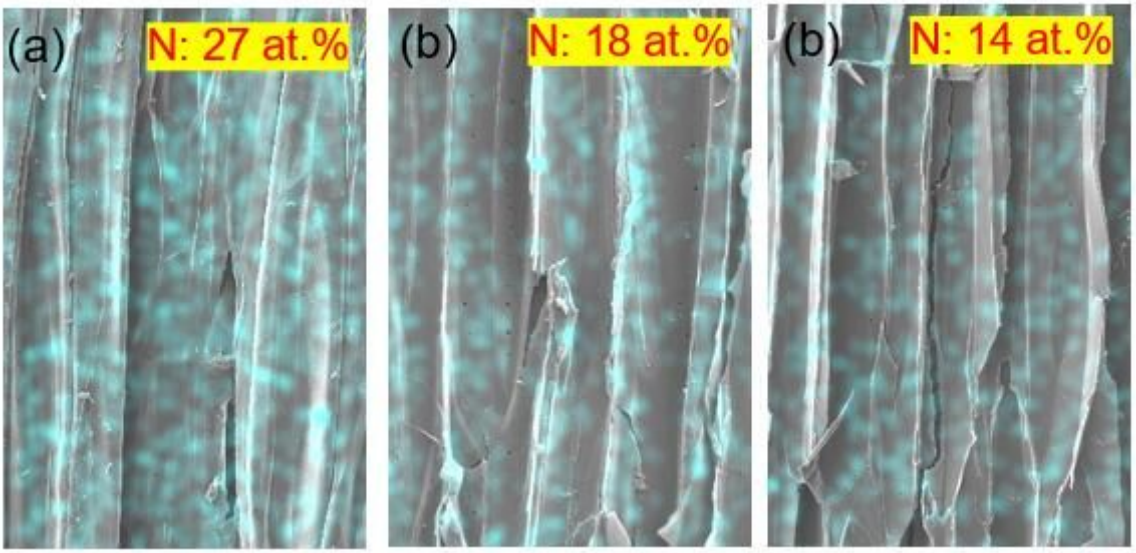

Figure S11. Nitrogen (N) EDX mapping of the conductive wood: (a) outer section, (b) middle section, and (c) inner section, demonstrating the PPy is distributed throughout the material.

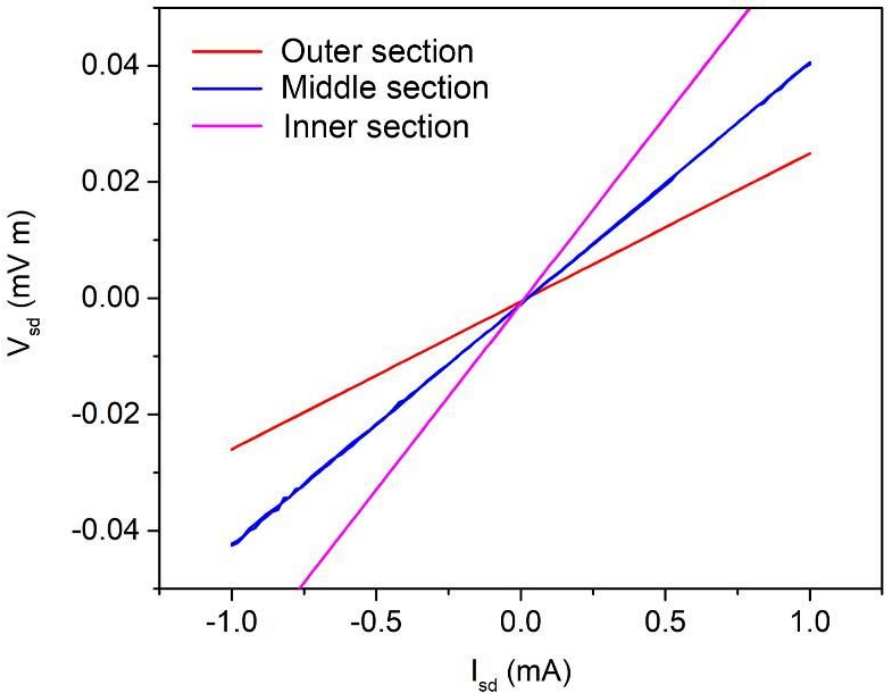

Figure S12. Normalized *I-V* curves of the outer, middle, and inner sections of the conductive wood.

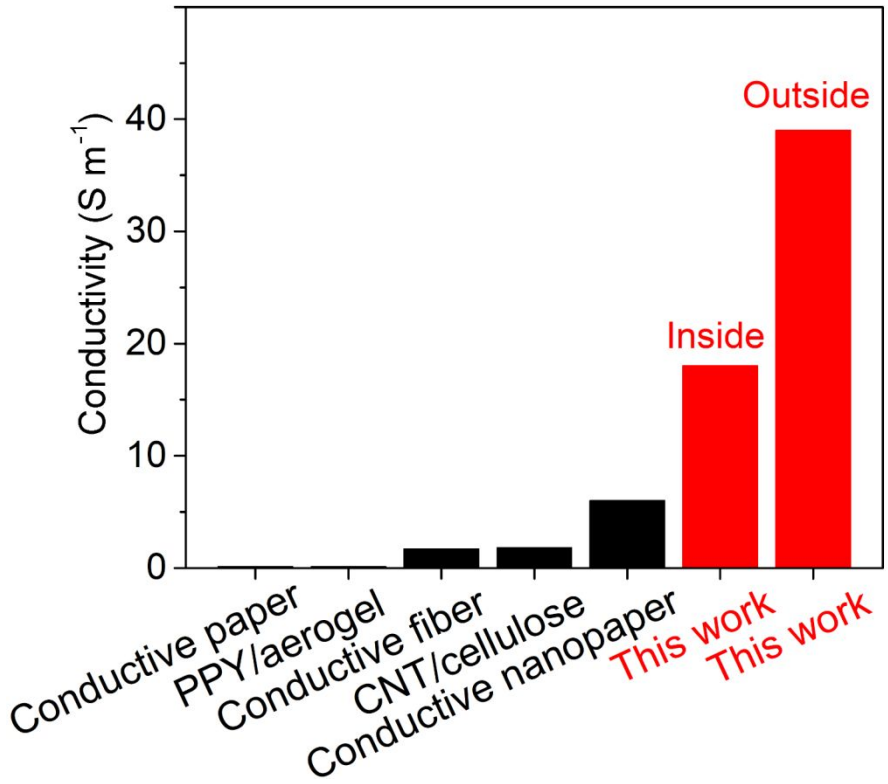

Figure S13. Comparison of the DC conductivity between the conductive wood and other conductive cellulose-based materials.[37, 38, 43-45]

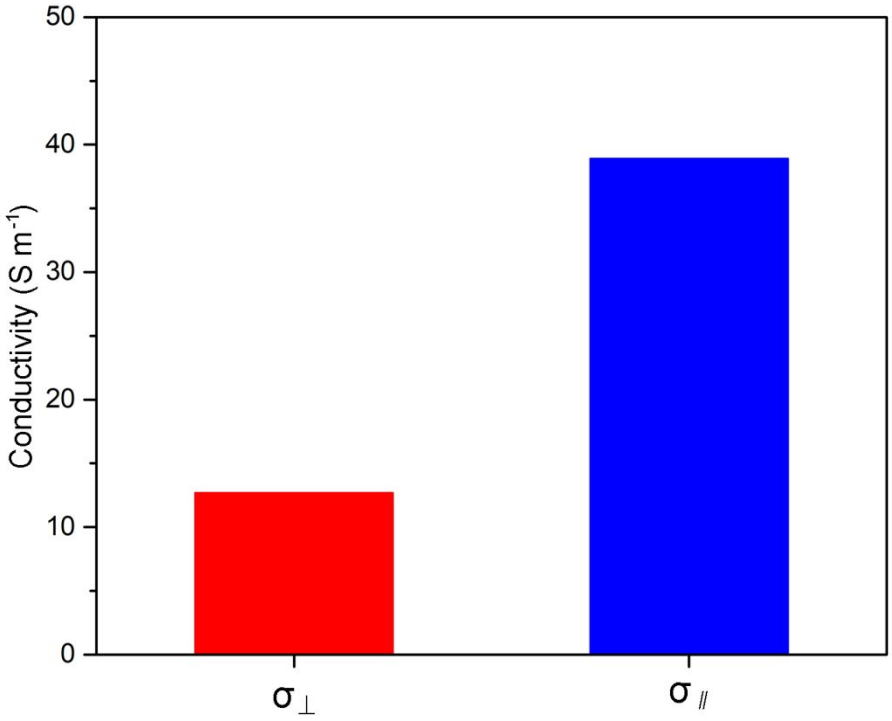

Figure S14. The conductivities perpendicular (σ⊥) and parallel (σ//) to the wood growth direction were 12 and 39 S m^{-1}, respectively, revealing the uniform electrical conductivity of the conductive wood.

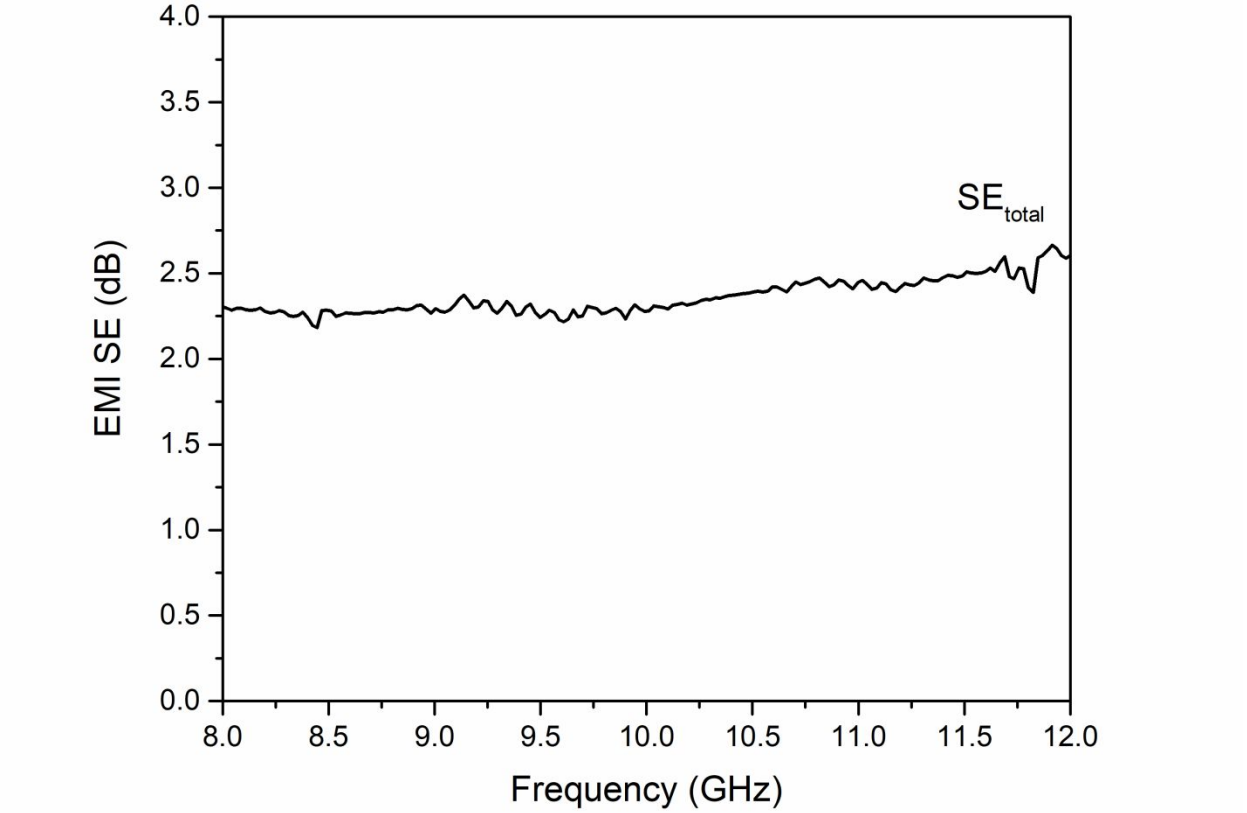

Figure S15. The low EMI shielding effectiveness (SE) of natural wood after the PPy coating suggests poor shielding performance.

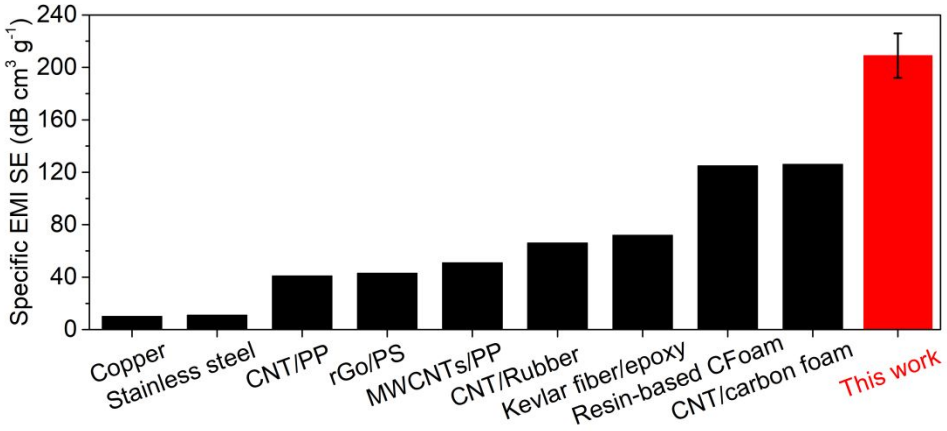

Figure S16. Comparison of the specific EMI performances of typical EMI shielding materials with good mechanical properties.[2-8] (CNT: carbon nanotubes; PP: polypropylene; PS: polystyrene; rGO: reduced graphene oxide; MWCNTs: multiwall carbon nanotubes; CFoam: carbon foams)

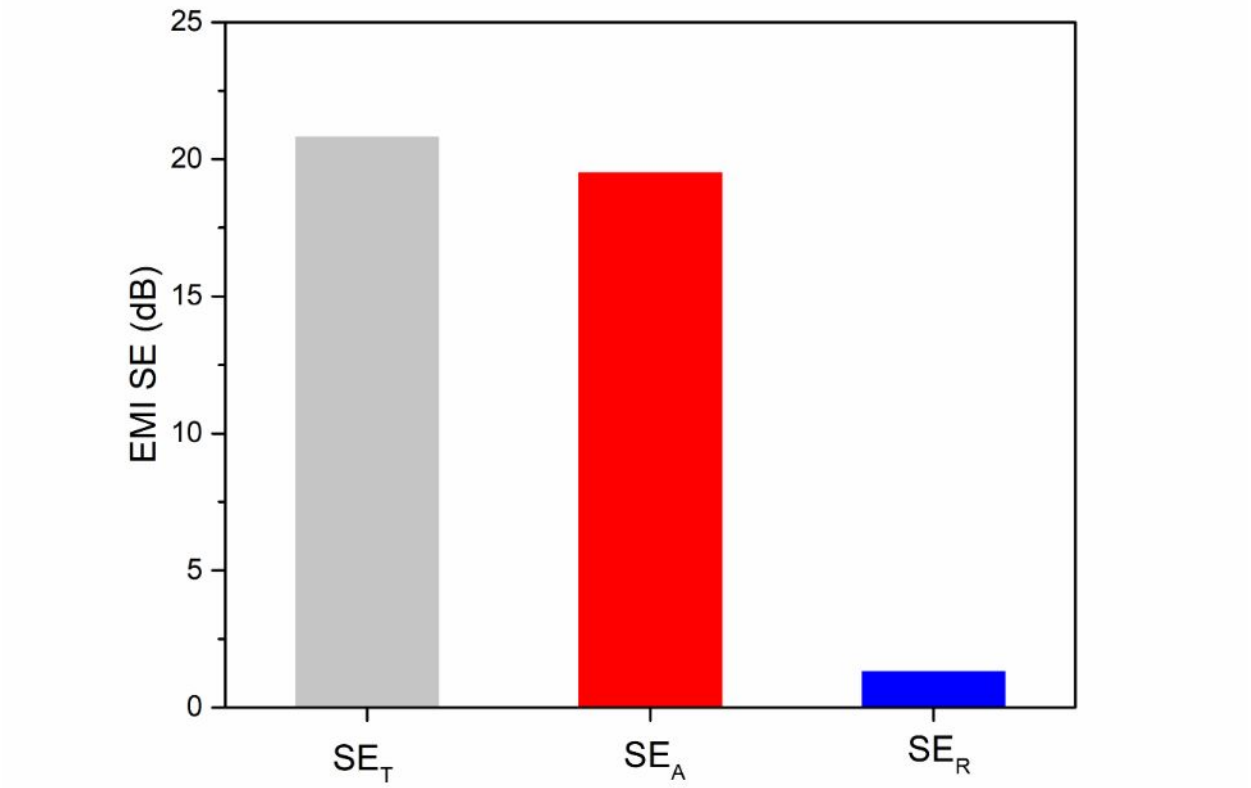

Figure S17. Total EMI shielding effectiveness (SE_T), absorption (SE_A), and reflection (SE_R) of conductive wood at the frequency of 8 GHz. The value of SE_A is much larger than that of SE_R, which suggests the conductive wood strongly absorbs electromagnetic radiation in the X-band region.

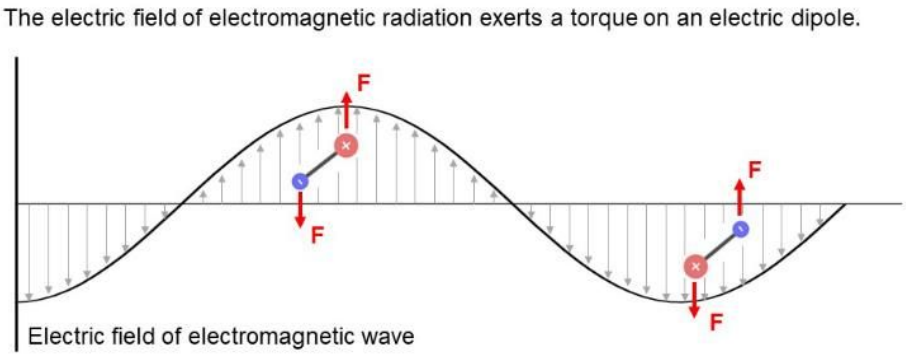

Figure S18. Schematic illustration of the electric dipole rotation under the electric field of electromagnetic radiation, demonstrating the absorption of electromagnetic wave which causes energy consumption due to the increased dipole rotational activity.

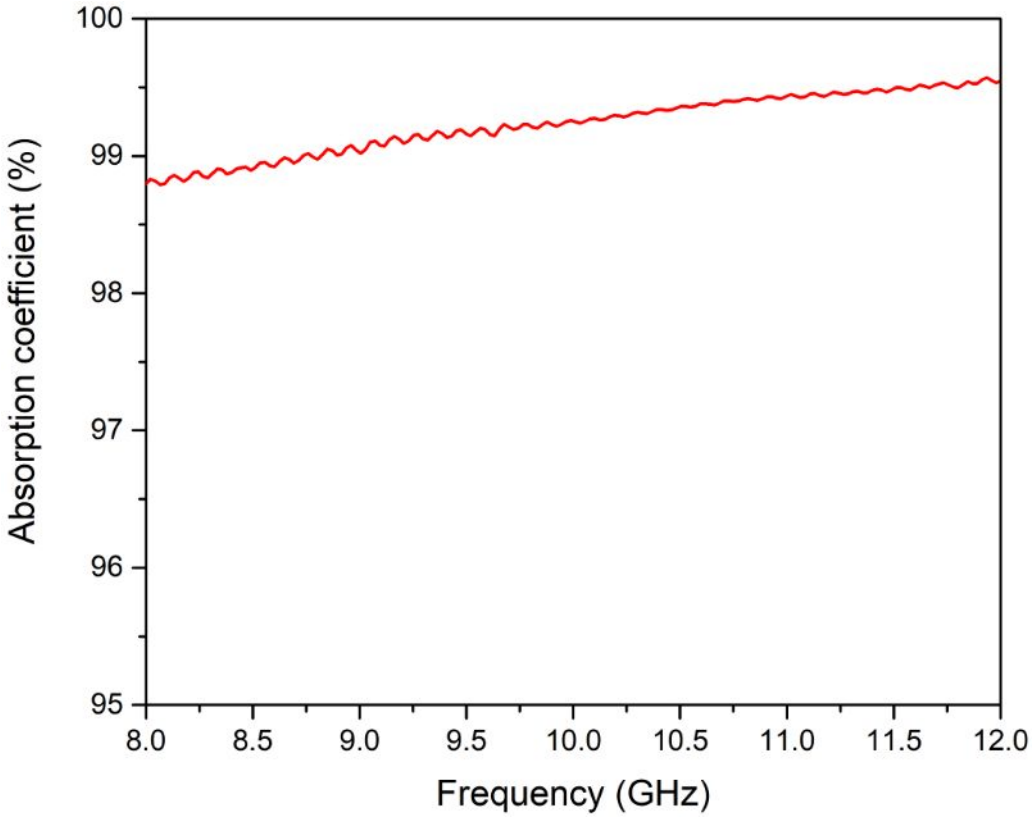

Figure S19. The high absorption coefficient of the conductive wood in the X-band range, indicating that adsorption dominated the attenuation mechanism.

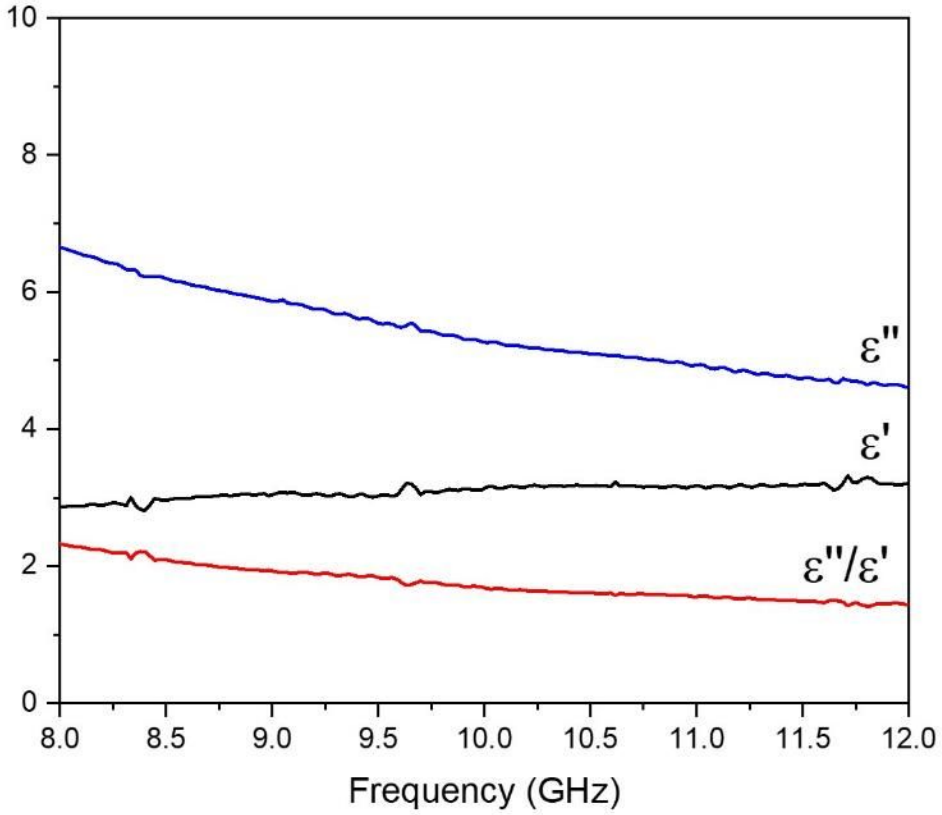

Figure S20. The complex permittivity and the ratio of ε″/ε′ for the conductive wood in the X-band range. The conductive wood with ε″/ε′ > 1 is considered a high loss material and can be effective in attenuating electromagnetic radiation.

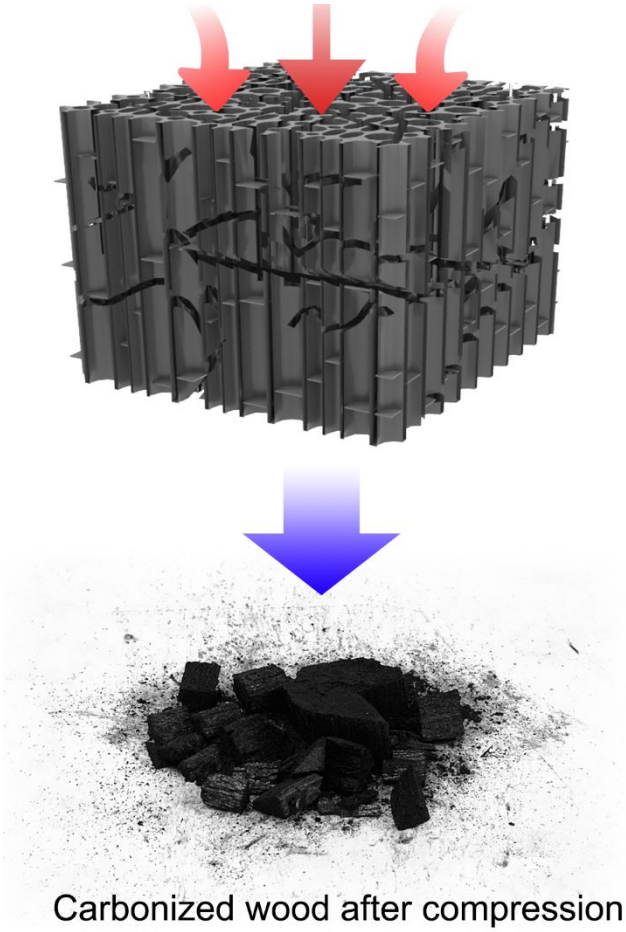

Figure S21. Schematic illustrations and photographs of the conductive wood after compressive tests.

References

(1) Ghasemi-Mobarakeh, L.; Semnani, D.;Morshed, M. A novel method for porosity measurement of various surface layers of nanofibers mat using image analysis for tissue engineering applications. *J. Appl. Polym. Sci.* **2007**, 106, 2536-2542.

(2) Yan, D. X.; Pang, H.; Li, B.; Vajtai, R.; Xu, L.; Ren, P. G.; Wang, J. H.; Li, Z. M. Structured reduced graphene oxide/polymer composites for ultra-efficient electromagnetic interference shielding. *Adv. Funct. Mater.* **2015,** *25*, 559-566.

(3) Verma, P.; Saini, P.; Choudhary, V. Designing of carbon nanotube/polymer composites using melt recirculation approach: effect of aspect ratio on mechanical, electrical and EMI shielding response. *Mater. Design* **2015**, 88, 269-277.

(4) Verma, P.; Saini, P.; Malik, R. S.; Choudhary, V. Excellent electromagnetic interference shielding and mechanical properties of high loading carbon-nanotubes/polymer composites designed using melt recirculation equipped twin-screw extruder. *Carbon* **2015**, 89, 308-317.

(5) Jia, L. C.; Yan, D. X.; Yang, Y.; Zhou, D.; Cui, C. H.; Bianco, E.; Lou, J.; Vajtai, R.; Li, B.; Ajayan, P. M.; Li, Z. M. High strain tolerant EMI shielding using carbon nanotube network stabilized rubber composite. *Adv. Mater. Technol.* **2017**, 2, 1700078.

(6) Kumar, R.; Dhakate, S. R.; Gupta, T.; Saini, P.; Singh, B. P.; Mathur, R. B. Effective improvement of the properties of light weight carbon foam by decoration with multi-wall carbon nanotubes. *J. Mater. Chem. A* **2013**, 1, 5727-5735.

(7) Micheli, D.; Vricella, A.; Pastore, R.; Delfini, A.; Giusti, A.; Albano, M.; Marchetti, M.; Moglie, F.; Primiani, V.M. Ballistic and electromagnetic shielding behaviour of multifunctional Kevlar fiber reinforced epoxy composites modified by carbon nanotubes. *Carbon* **2016**, 104, 141-156.

(8) Kumar, R.; Singh, A.P.; Chand, M.; Pant, R.P.; Kotnala, R.K.; Dhawan, S.K.; Mathur, R.B.; Dhakate, S.R. Improved microwave absorption in lightweight resin-based carbon foam by decorating with magnetic and dielectric nanoparticles. *RSC Adv.* **2014**, 4, 23476-23484.